metals

MDPI

Article

Effects of Various Heat Treatments on Room- and High-Temperature Tensile Properties of Ti65 Alloy Fabricated via Electron Beam Powder Bed Fusion

Yinling Jin [1,*], Yanmei Liu [1], Xingwang Zhao [1], Feng Guan [1], Chengjie Huang [1], Yu Zhang [2], Jingling Zhang [2], Yufeng Ding [2] and Xiaoyu Liang [3]

[1] Shenyang Aircraft Corporation, Shenyang 110850, China
[2] Beijing Quick Beam Technology Co., Ltd., Beijing 100176, China
[3] Department of Mechanical Engineering, Tsinghua University, Beijing 100084, China
* Correspondence: hitjinyinling@163.com

Abstract

Ti65 is a promising structural material for lightweight high-temperature aerospace components, yet the heat-treatment response of Ti65 fabricated by electron beam powder bed fusion (EB-PBF) remains insufficiently understood. In this study, EB-PBF Ti65 specimens were subjected to solution treatments at 800–1000 °C for different holding times followed by aging at 650 °C for 2–8 h. Microstructural evolution was characterized and tensile properties were evaluated at room temperature and 650 °C along the XY and Z directions. The as-built alloy exhibited a fine basketweave α + β lamellar microstructure with evident anisotropy. Increasing the solution temperature promoted α-lamella dissolution, elemental homogenization, discontinuity of grain-boundary α, and microstructural reconstruction. The 1000 °C/2 h + 650 °C/2 h treatment significantly improved room-temperature strength and transverse ductility, giving ultimate tensile strengths of approximately 1050 MPa and reducing anisotropy. At 650 °C, all specimens showed reduced strength but increased ductility; low-temperature solution treatment favored ductility, whereas 1000 °C-based treatments combined with appropriate aging improved elevated-temperature strength. Aging for 4 h provided a balanced strength–ductility combination, while longer aging enhanced yield strength but reduced ductility. These results demonstrate that tailoring solution and aging parameters is essential for optimizing the microstructure and mechanical performance of EB-PBF Ti65 alloy. Specifically, the 1000 °C/2 h + 650 °C/2–4 h regime achieved UTS of ~1050 MPa at room temperature and ~608 MPa at 650 °C, with XY-direction elongation increasing from 5.4% to 11.5%, representing a quantitative anisotropy reduction of approximately 53%.

Keywords: electron beam powder bed fusion; heat treatment; Ti65 Alloy; tensile property

Check for updates

Academic Editor: Abdollah Saboori

Received: 15 June 2026
Revised: 21 July 2026
Accepted: 5 August 2026
Published: 14 September 2026

Copyright: © 2026 by the authors. Licensee MDPI, Basel, Switzerland. This article is an open access article distributed under the terms and conditions of the Creative Commons Attribution (CC BY) license.

1. Introduction

Titanium alloys are critical lightweight high-temperature structural materials applied in aero-engine compressor disks, blades, casings, and aerospace hot-section structural components [1,2]. Compared to nickel-based superalloys, titanium alloys possess lower density and higher specific strength, exhibiting significant weight reduction advantages in the medium-to-high temperature range. However, the high-temperature service capability of titanium alloys is constrained by multiple factors, including α-phase stability,

β-phase fraction, silicide precipitation, grain boundary morphology, and oxidation behavior. Balancing strength, ductility, and microstructural stability at elevated service temperatures remains a core issue in the design and manufacturing of high-temperature titanium alloys [3]. As a 600 °C-class near-α high-temperature titanium alloy, the Ti65 alloy achieves solid solution strengthening, precipitation strengthening, and thermal stabilization through multi-element alloying, and is thus considered a crucial candidate material for high-temperature load-bearing structures in the aerospace industry.

Complex high-temperature titanium alloy components typically feature thin walls, irregular profiles, internal cavities, or monolithic characteristics. When fabricated using conventional forging, rolling, and machining processes, these components often suffer from prolonged manufacturing cycles, substantial material waste, and limited structural degrees of freedom. Considering the limitations of conventional processing methods, researchers have begun to explore the fabrication of Ti65 alloy using additive manufacturing techniques [4–6]. As an advanced powder bed additive manufacturing technology, Electron Beam Powder Bed Fusion (EB-PBF) enables the direct fabrication of complex metallic components in a vacuum environment. Its high-temperature preheating characteristic not only improves powder bed stability but also reduces thermal stress and crack susceptibility, making it particularly suitable for the fabrication of titanium alloys and other highly reactive metallic materials. For highly alloyed and high-temperature strengthened titanium alloys such as Ti65, EB-PBF is expected to overcome the limitations of traditional manufacturing methods in preparing complex structures, thereby enabling the short-process manufacturing of high-performance complex components [7].

Recent studies on EB-PBF fabricated near-alpha titanium alloys have demonstrated that post-processing heat treatments significantly influence microstructural homogenization, phase transformation behavior, and mechanical property optimization. For instance, Li et al. [8] investigated sub-transus cyclic heat treatment effects on laser-deposited Ti65 alloys, revealing improved microstructural uniformity through controlled alpha-phase dissolution and reprecipitation. Zhao et al. [9] examined variant selection mechanisms in Ti65 under different cooling rates, highlighting the importance of thermal history on final alpha-phase morphology.

Heat treatment is one of the most critical processing steps in the microstructural tailoring of high-temperature titanium alloys [8–11]. The beta-transus temperature of Ti65 alloy was determined to be approximately 1010 °C based on differential scanning calorimetry (DSC) analysis, consistent with previously reported values for this alloy system. For the Ti65 alloy, heat treatment is not only associated with residual stress relief but also directly determines the α-phase size, secondary α precipitation, β-phase retention, grain boundary α continuity, and the extent of elemental segregation elimination [12]. An elevated solution temperature facilitates the dissolution of the primary α phase and elemental diffusion, transforming the continuous grain boundary α phase in the as-built state into a discontinuous distribution, and inducing the formation of a bimodal microstructure characterized by the coexistence of primary and secondary α phases [13]. Within this microstructure, the coarse primary α phase enhances deformation compatibility, while the fine secondary αphase improves strength, thereby facilitating an optimal combination of room-temperature strength and ductility. On the other hand, aging treatment stabilizes the phase composition and regulates precipitation behavior; however, an excessive aging duration may lead to the over-precipitation of the α phase or a reduction in the β phase, consequently impairing high-temperature strength [14]. Therefore, the optimization of heat treatment regimes necessitates a balance between room-temperature and 650 °C elevated-temperature tensile properties, rather than relying solely on a single performance indicator as the criterion. Sun et al. [15,16] systematically evaluated the microstructural evolution and mechanical properties of additively manufactured Ti65 alloys

after various annealing treatments, establishing correlations between processing parameters, microstructural features, and tensile behavior.

Currently, although research on laser additive manufacturing of the Ti65 alloy has been reported [15,16], studies focusing on the microstructural evolution during heat treatment and the correlation between room- and elevated-temperature properties of the Ti65 alloy fabricated by EB-PBF remain relatively scarce. In particular, the mechanisms by which different solution temperatures, solution durations, and aging times influence the α-phase morphology, grain boundary α-phase state, and elevated-temperature tensile behavior require further elucidation [17,18]. Research on Ti-6Al-4V and Ti-5Al-5V-5Mo-3Cr alloys fabricated by EB-PBF has also shown that solution treatment below the beta-transus temperature effectively reduces mechanical anisotropy by disrupting continuous grain-boundary alpha phases and promoting bimodal microstructure formation [19,20]. These studies collectively underscore that optimizing heat-treatment regimes is crucial for achieving balanced strength-ductility combinations and minimizing anisotropy in additively manufactured high-temperature titanium alloys.

Investigating these aspects not only contributes to a deeper understanding of the phase transformation behavior of high-temperature titanium alloys under the unique thermal history of electron beam additive manufacturing but also provides a processing foundation for the performance stabilization of complex components. Therefore, this study focuses on the EB-PBF Ti65 alloy to investigate the effects of various heat treatment regimes on its microstructure and tensile properties. Emphasis is placed on analyzing the roles of solution temperature, solution duration, and aging time in determining the α-phase size, the formation of bimodal microstructures, the discontinuity of grain boundary α, and elemental homogenization. This paper aims to provide a reference for optimizing the post-processing regimes of the EB-PBF Ti65 alloy and to facilitate the engineering application of high-temperature complex components.

2. Materials and Methods

2.1. Sample Preparation

Gas-atomized spherical Ti65 alloy powder was utilized as the raw material in this study, supplied by Xi'an Bright Laser Technologies Co., Ltd. (BLT, Xi'an, China). Chemical composition analysis (Table 1) indicated that the contents of the principal alloying elements fell within the nominal design range. Specifically, the oxygen (O) content of the powder was approximately 0.08 wt.%, which satisfied the stringent oxygen control requirements of this study and demonstrated the absence of significant oxidation contamination. The particle size distribution was determined via laser diffraction analysis, yielding D_{10}, D_{50}, D_{90} values of approximately 60.46 μm, 80.60 μm, and 107.69 μm, respectively. This size distribution matches the powder-spreading characteristics required for the Electron Beam Powder Bed Fusion process. The Hall flowability of the powder was measured at 28.04 s/50 g, and the apparent density was 2.58 g/cm^3.

The Ti65 alloy specimens were fabricated using a Qbeam-E200 Electron Beam Powder Bed Fusion system from Beijing Quick Beam Technology Co., Ltd. (Qbeam, Beijing, China). The entire fabrication process was carried out in a vacuum environment. To prevent powder scattering (commonly known as the "smoke" effect) during the powder-spreading and melting stages, the build plate was preheated prior to fabrication. The preheating area of the build plate was 200 mm × 200 mm, and the preheating duration was 40 min. Following the deposition of each powder layer, powder bed preheating was conducted to induce a weakly sintered state within the powder, thereby enhancing the stability of the powder bed. The powder bed preheating strategy employed a combination of zonal scanning and localized preheating. The hatch spacing was set to 0.1 mm. The melting and hatching

process adopted a typical scan vector length parameter interpolation method. The specific process parameters are detailed in Table 2.

Table 1. Chemical composition of the Ti65 powder (wt.%).

Element	Nominal Composition (wt.%)	Measured Composition (wt.%)
Ti	Bal.	Bal. *
Al	5.5–6.5	5.798
Mo	0.2–1.0	0.464
Zr	2.0–4.0	3.227
Sn	3.0–4.5	3.582
W	0.5–1.5	0.694
Si	0.2–0.5	0.375
Fe	–	0.033
Ta	0.5–2.5	0.814
Nb	0.2–1.0	0.348
C	0.02–0.08	0.050
N	≤0.05	0.007
Ni	≤0.05	0.008
H	≤0.01	0.0014
O	≤0.08	0.080

Note: All values are given in wt.%. * The balance (Bal.) Ti content was calculated by difference from the measured concentrations of the other alloying elements.

Table 2. EB-PBF process parameters to fabricate the Ti65 specimens.

Line Length	Hatch Spacing	Accelerating Voltage	Beam Current	Scanning Velocity	Layer Thickness
15 mm	0.1 mm	60 kV	7.4 mA	1.2 m/s	0.075 mm

To investigate the effects of heat treatment regimes on the microstructure and properties of the EB-PBF Ti65 alloy, heat treatment schemes comprising varying solution temperatures, solution durations, and aging times were designed. All the employed heat treatments are summarized in Table 3. A vacuum heat treatment furnace was employed for all heat treatment procedures. Initially, experiments evaluating different solution temperatures were conducted; the specimens were solution-treated at 800, 900, and 1000 °C for a constant holding time of 2 h, followed by an aging treatment at 650 °C for 2 h. To further examine the influence of solution duration, the holding time was extended to 4 h at a fixed solution temperature of 1000 °C, while maintaining the identical aging regime (650 °C/2 h). Finally, after establishing 1000 °C/2 h as the primary solution regime, the aging duration at 650 °C was systematically varied, specifically set to 2, 4, 6, and 8 h. All heat-treated specimens were subjected to air cooling (AC). These designed heat treatment regimes facilitate a systematic analysis of the effects of primary α-phase dissolution, secondary α-phase precipitation, grain boundary α-phase discontinuity, and elemental homogenization on the tensile properties. The selection of 800, 900, and 1000 °C as solution temperatures was based on the following rationale: 800 °C represents a relatively low sub-transus temperature intended to evaluate the effects of recovery and stress relief while preserving the original fine lamellar microstructure; 900 °C was chosen as an intermediate temperature to examine partial alpha-phase dissolution and initial microstructural reconstruction; and 1000 °C, which is slightly below the beta-transus temperature (~1010 °C), was selected to promote significant alpha-phase dissolution, grain-boundary alpha discontinuity, and bimodal microstructure formation without inducing excessive beta-grain growth. The aging temperature of 650 °C was determined based on the typical service temperature of Ti65 alloy and previous studies on near-alpha titanium alloys, which indicate that aging

at 600–700 °C facilitates secondary alpha-phase precipitation and silicide formation while maintaining microstructural stability [8,13].

Table 3. Heat treatments for Ti65 alloys.

No.	Heat Treatment
1	800 °C/2 h + 650 °C/2 h
2	900 °C/2 h + 650 °C/2 h
3	1000 °C/2 h + 650 °C/2 h
4	1000 °C/4 h + 650 °C/2 h
5	1000 °C/2 h + 650 °C/4 h
6	1000 °C/2 h + 650 °C/6 h
7	1000 °C/2 h + 650 °C/8 h

To evaluate the mechanical anisotropy and heat treatment response of the material, tensile specimens in both the XY- and Z-directions were prepared. Specifically, the tensile axis of the Z-direction specimens was parallel to the build direction (BD), whereas that of the XY-direction specimens was perpendicular to the BD. The specimens were initially fabricated as plate-like blanks via Electron Beam Powder Bed Fusion (EB-PBF), as illustrated in Figure 1a,b. Subsequently, each as-built plate was sectioned using wire electrical discharge machining (WEDM) and machined into standard tensile specimens, as depicted in Figure 1c,d. Mechanical machining was employed to prepare the tensile specimens, thereby eliminating the detrimental effects of the rough as-built surfaces and near-surface defects on the testing results. To ensure the comparability of test results across various heat treatment regimes, all specimens, regardless of their pre- or post-heat treatment status, were uniformly machined in accordance with identical dimensional specifications. Samples for microstructural characterization were extracted from regions adjacent to the tensile specimens or from companion samples subjected to the same furnace cycle. The observation planes primarily encompassed cross-sections perpendicular and parallel to the build direction, facilitating the analysis of columnar grains, α lamellae, and grain boundary α-phase characteristics.

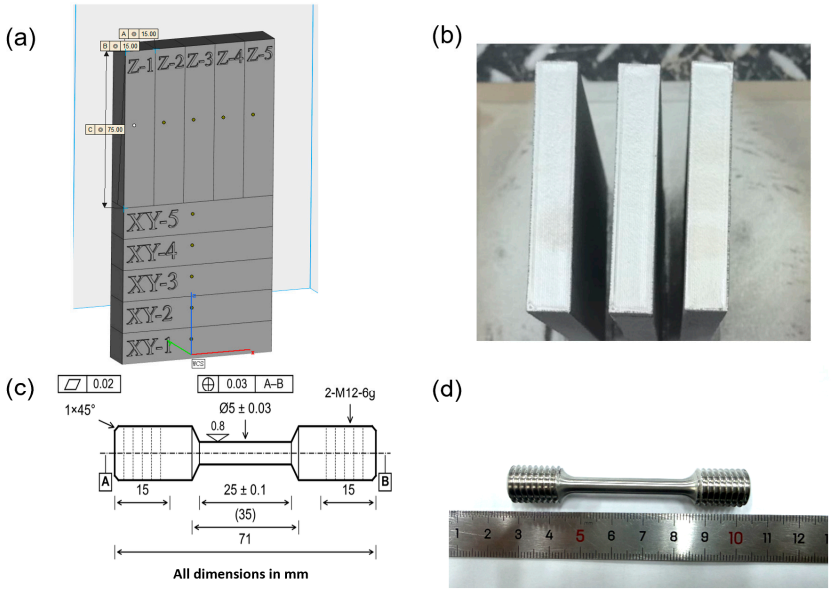


Figure 1. (**a**) CAD model of the Ti65 alloy build, indicating the extraction locations of the Z- and XY-direction tensile specimens; (**b**) photograph of the as-built blocks; (**c**) dimensional drawing of the room-temperature and 650 °C tensile specimens; (**d**) photograph of the machined room-temperature and 650 °C tensile specimens.

2.2. Characterization and Testing Methods

Microstructural characterization was conducted using optical microscopy (OM) and scanning electron microscopy (SEM). Metallographic samples were extracted via wire electrical discharge machining (WEDM), followed by sequential mounting, grinding with SiC abrasive papers, mechanical polishing, and chemical etching. The etched specimens were utilized to observe the α -phase morphology, prior α grains, grain boundary α phase, and overall microstructural homogeneity. SEM was primarily employed to further analyze the α/β lamellar structures, fracture morphologies, and localized defect characteristics. Furthermore, energy-dispersive X-ray spectroscopy (EDS) was utilized to ascertain the elemental distribution profiles of Mo, W, Ta, Si, Zr, and Nb within the α phase, β phase, and localized precipitates.

Room-temperature (RT) tensile testing was conducted under ambient conditions. The evaluated mechanical metrics included ultimate tensile strength (UTS), yield strength (YS), and elongation at fracture (EL). For each heat-treatment condition and testing direction (XY and Z), a minimum of two tensile specimens were tested to ensure statistical reliability. The reported values represent the mean plus or minus standard deviation (SD) of the tested specimens. High-temperature tensile tests were performed at 650 °C. The specimens were held at the target temperature until thermal equilibrium was reached prior to load application. This was designed to evaluate the strength retention capability and plastic deformation behavior of the Ti65 alloy at its typical service temperature.

3. Results

3.1. Microstructure Observations

The as-built Ti65 alloy fabricated by Electron Beam Powder Bed Fusion (EB-PBF) primarily consists of a typical basketweave α + β lamellar microstructure. In the as-built state (Figure 2a), the α lamellae are relatively fine and distributed in an interlaced manner, with localized regions exhibiting certain colony-like orientation features.

After the 800 °C/2 h + 650 °C/2 h treatment (Figure 2b), the morphological features remain similar to the as-built state, with the α lamellae remaining fine and dense, and much of the original lamellar microstructure being retained.

Following the 900 °C/2 h + 650 °C/2 h treatment (Figure 2c), the lamellar α phase undergoes slight coarsening, and the lamellar boundaries become more distinct. A fraction of the fine α phase dissolves and reprecipitates, while the overall basketweave architecture is maintained.

After the 1000 °C/2 h + 650 °C/2 h treatment (Figure 2d), the α lamellae exhibit pronounced growth, resulting in an increased interlamellar spacing and the localized formation of coarser lamellar colonies. Consequently, the microstructure displays more obvious reconstruction features, with enhanced phase contrast.

When the solution duration is extended to 1000 °C/4 h + 650 °C/2 h (Figure 2e), further coarsening of the lamellae is observed, accompanied by localized microstructural heterogeneity.

Upon extending the 650 °C aging time following the 1000 °C/2 h solution treatment, all corresponding specimen groups (Figure 2f–h) retain the basketweave α + β microstructure. As the aging time increases from 4 h to 8 h, the α lamellae gradually coarsen, the interlamellar β phase becomes stabilized, and the microstructural contrast becomes more pronounced.

Overall, following the high-temperature solution and aging treatments, the microstructure of the Ti65 alloy evolves from fine, dense as-built lamellae into a more stable and coarsened α + β basketweave architecture, with the 1000 °C solution treatment exerting the most significant regulatory effect on the microstructure.

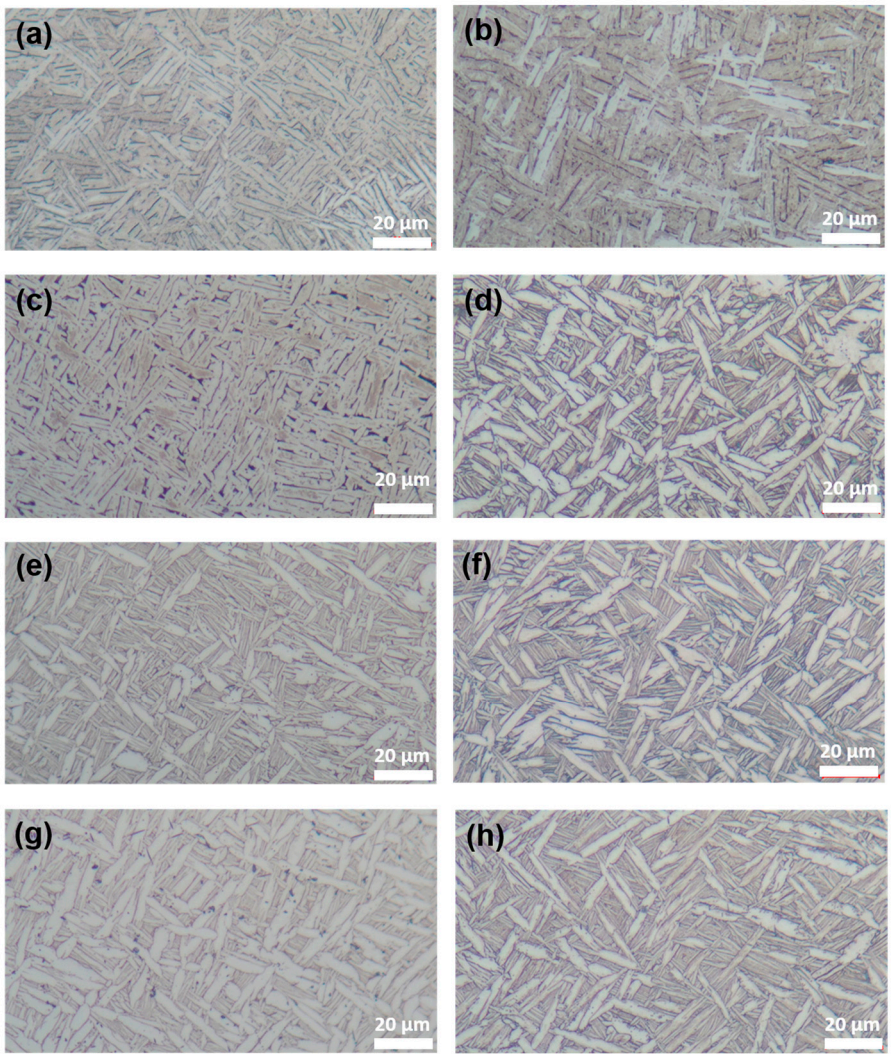


Figure 2. Optical micrographs of the EB-PBF-fabricated Ti65 alloy subjected to various heat treatment regimes (all taken from lateral cross-sections): (**a**) as-built state; (**b**) 800 °C/2 h + 650 °C/2 h; (**c**) 900 °C/2 h + 650 °C/2 h; (**d**) 1000 °C/2 h + 650 °C/2 h; (**e**) 1000 °C/4 h + 650 °C/2 h; (**f**) 1000 °C/2 h + 650 °C/4 h; (**g**) 1000 °C/2 h + 650 °C/6 h; (**h**) 1000 °C/2 h + 650 °C/8 h. The corresponding lower-magnification micrographs are provided in Figure S1 of the Supporting Information.

As evidenced by the SEM micrographs, distinct variations in phase morphology, lamellar scale, and precipitation behavior are observed in the Ti65 alloy subjected to different heat treatments. In the as-built state (Figure 3a), the bright-white α lamellae are fine and densely distributed, exhibiting a narrow interlamellar spacing. Short rod-like and discontinuous α-phase morphologies are locally observable.

Following the 800 °C/2 h + 650 °C/2 h treatment (Figure 3b), the original fine lamellae are largely retained. After the 900 °C/2 h + 650 °C/2 h treatment (Figure 3c), an abundance of fine granular precipitates emerges between the lamellae, which are likely secondary α phase or fine precipitates enriched with Si and refractory elements.

Upon the 1000 °C/2 h + 650 °C/2 h treatment (Figure 3d), the boundaries of the lamellar colonies become highly distinct. Partial dissolution, fragmentation, and reprecipitation of the α lamellae occur, yielding a microstructural coexistence of coarse lamellae and fine precipitates. When the solution duration is extended to 1000 °C/4 h (Figure 3e), the coarse lamellae and broadened transformed β regions become more pronounced, accompanied by a reduction in fine precipitates.

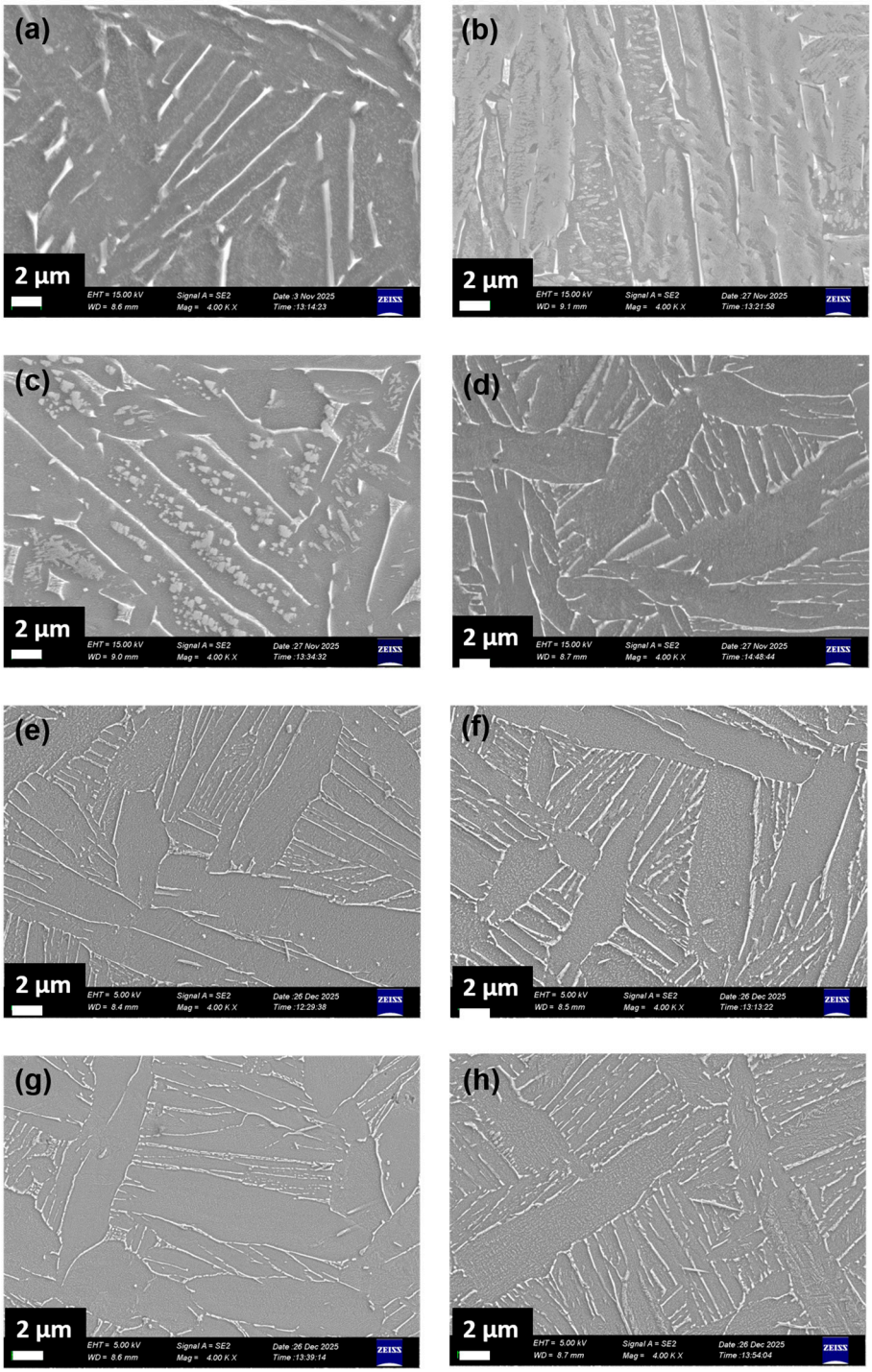


Figure 3. SEM micrographs of the EB-PBF-fabricated Ti65 alloy subjected to various heat treatment regimes (all taken from lateral cross-sections): (**a**) as-built state; (**b**) 800 °C/2 h + 650 °C/2 h; (**c**) 900 °C/2 h + 650 °C/2 h; (**d**) 1000 °C/2 h + 650 °C/2 h; (**e**) 1000 °C/4 h + 650 °C/2 h; (**f**) 1000 °C/2 h + 650 °C/4 h; (**g**) 1000 °C/2 h + 650 °C/6 h; (**h**) 1000 °C/2 h + 650 °C/8 h. The corresponding lower-magnification micrographs are provided in Figure S2 of the Supporting Information.

Regarding the extension of the 650 °C aging time following the 1000 °C/2 h solution treatment: in Figure 3f, the fine secondary α phase precipitates adequately, with dense, short lath-like precipitates visible between the lamellae; in Figure 3g, the precipitates continue to grow and tend to become continuous, with localized coarsening and agglomeration observed; in Figure 3h, the lamellar morphology remains relatively stable, but partial coalescence of fine precipitates occurs, leading to an increased interlamellar spacing.

3.2. Tensile Properties

3.2.1. Room Temperature Tensile Tests and Fracture Surface Observations

After various heat treatments, the room-temperature and 650 °C tensile properties of the EB-PBF Ti65 alloy changed significantly and exhibited pronounced anisotropy. The room-temperature and elevated-temperature tensile properties of different specimens are summarized in Table 4 and are plotted in Figure 4.

Table 4. Data from tensile tests of the EB-PBF Ti65 alloy under different heat-treatment conditions at room temperature, including yield strength, ultimate tensile strength, and elongation.

Heat Treatment Conditions	Building Direction	UTS (MPa)	YS (MPa)	Elongation (%)
As-built	XY	972	887	5.8
As-built	XY	959	882	5
As-built	Z	989	903	13.2
As-built	Z	971	885	13
800 °C/2 h + 650 °C/2 h	Z	989	895	14
800 °C/2 h + 650 °C/2 h	Z	985	888	17.6
800 °C/2 h + 650 °C/2 h	XY	975	900	6.3
800 °C/2 h + 650 °C/2 h	XY	976	899	4.1
900 °C/2 h + 650 °C/2 h	Z	1004	905	15.6
900 °C/2 h + 650 °C/2 h	Z	1007	904	17.1
900 °C/2 h + 650 °C/2 h	XY	1002	923	6.1
900 °C/2 h + 650 °C/2 h	XY	997	927	4.4
1000 °C/2 h + 650 °C/2 h	Z	1047	963	14.2
1000 °C/2 h + 650 °C/2 h	Z	1053	948	11.5
1000 °C/2 h + 650 °C/2 h	XY	1052	951	9.2
1000 °C/2 h + 650 °C/2 h	XY	1050	943	13.8
1000 °C/4 h + 650 °C/2 h	Z	1036	946	14.4
1000 °C/4 h + 650 °C/2 h	Z	1047	952	12.9
1000 °C/4 h + 650 °C/2 h	XY	1054	961	8
1000 °C/4 h + 650 °C/2 h	XY	1047	953	10.6
1000 °C/2 h + 650 °C/4 h	Z	1044	964	11.8
1000 °C/2 h + 650 °C/4 h	Z	1055	968	9.6
1000 °C/2 h + 650 °C/4 h	XY	1069	983	10.4
1000 °C/2 h + 650 °C/4 h	XY	1055	970	11.4
1000 °C/2 h + 650 °C/6 h	Z	1047	962	7.8
1000 °C/2 h + 650 °C/6 h	Z	1052	974	10
1000 °C/2 h + 650 °C/6 h	XY	1066	989	9.4
1000 °C/2 h + 650 °C/6 h	XY	1059	978	8.2
1000 °C/2 h + 650 °C/8 h	Z	1044	966	8.8
1000 °C/2 h + 650 °C/8 h	Z	1044	955	11.5
1000 °C/2 h + 650 °C/8 h	XY	1068	987	9.4
1000 °C/2 h + 650 °C/8 h	XY	1054	973	9.8

At room temperature, the as-built specimen exhibited an ultimate tensile strength (UTS) of approximately 966 MPa and a yield strength (YS) of approximately 884 MPa in the XY direction, while the elongation was only about 5.4%. In contrast, the Z-direction specimen showed better ductility, with an elongation of approximately 13.1%. After heat treatment at 800 °C/2 h + 650 °C/2 h, the strength remained essentially unchanged, while the Z-direction elongation increased to approximately 15.8%; however, the XY-direction elongation remained low, at about 5.2%. After 900 °C/2 h + 650 °C/2 h treatment, the strength increased and the Z-direction elongation reached approximately 16.4%, whereas the improvement in XY-direction ductility was still limited. After 1000 °C/2 h + 650 °C/2 h treatment, the overall mechanical properties were significantly enhanced. The UTS values in both the XY and Z directions were approximately 1050 MPa, the YS of XY and Z directions

were 947 MPa and 956 MPa, and the XY-direction elongation increased to approximately 11.5% and the Z-direction elongation was 12.9%. When the solution holding time was extended to 4 h, the strength was largely retained, but the XY-direction ductility decreased slightly. Prolonging the aging time at 650 °C maintained a high strength level. Among these conditions, aging for 4 h provided a better strength–ductility balance, whereas aging for 6 h further increased the yield strength but reduced the elongation to approximately 9%.

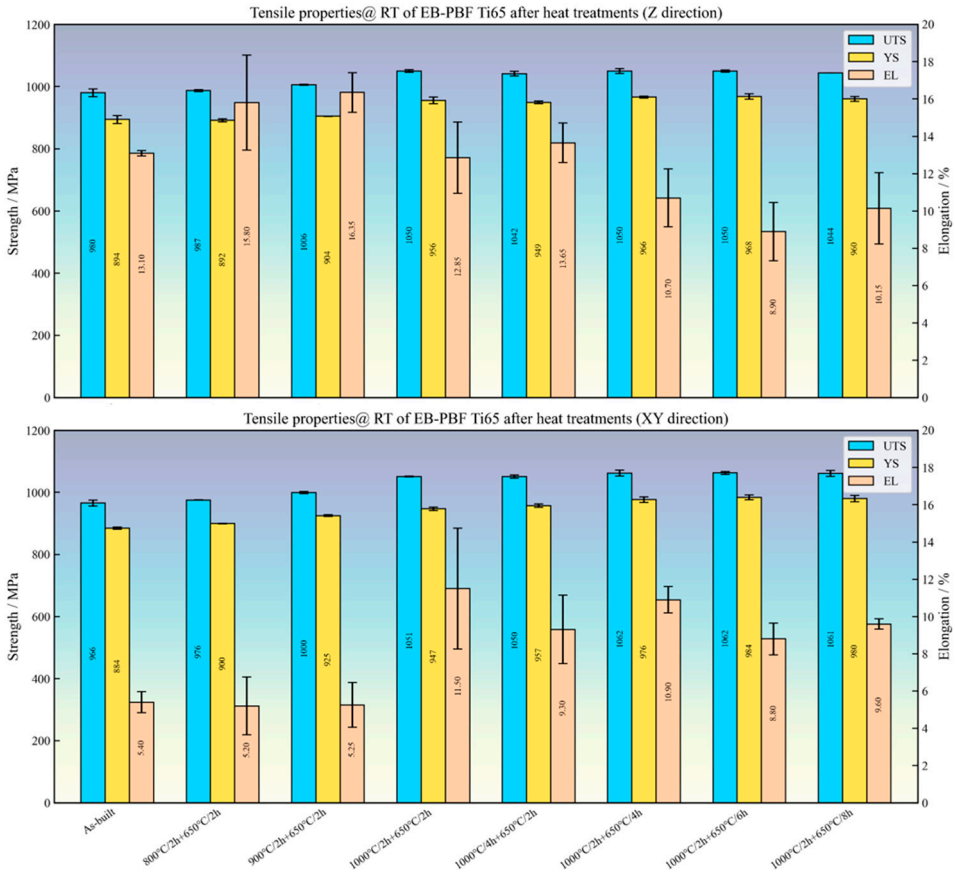


Figure 4. Tensile properties of the EB-PBF Ti65 alloy under different heat-treatment conditions at room temperature, including yield strength, ultimate tensile strength, and elongation.

The room-temperature tensile fracture surfaces of specimens subjected to solution heat treatment at 900 °C, which exhibit similarities to those treated at 800 °C, are provided in Figure S3 of the Supporting Information. As shown in Figure S3a–c, the XY-oriented specimens display intergranular brittle fracture at room temperature. The macroscopic surface features numerous columnar grain boundaries, with relatively few dimples, along with some cleavage facets and void defects. In contrast, as depicted in Figure S3d–f, the Z-oriented specimens exhibit transgranular ductile fracture, characterized by abundant dimples on the fracture surface, accompanied by partial cleavage facets and void defects.

Figure 5 presents the room-temperature tensile fracture surfaces of specimens after solution heat treatment at 1000 °C. As illustrated in Figure 5a–c, the macroscopic surface of the XY-oriented specimens shows a significant reduction in columnar grain boundaries. The microscopic fracture morphology consists of tear ridges and dimples, with some cleavage facets and void defects, indicating a ductile fracture mode. As shown in Figure 5d–f, the Z-oriented specimens also undergo transgranular ductile fracture, where the fracture surface microstructure comprises tear ridges and dimples, alongside partial cleavage facets and void defects.

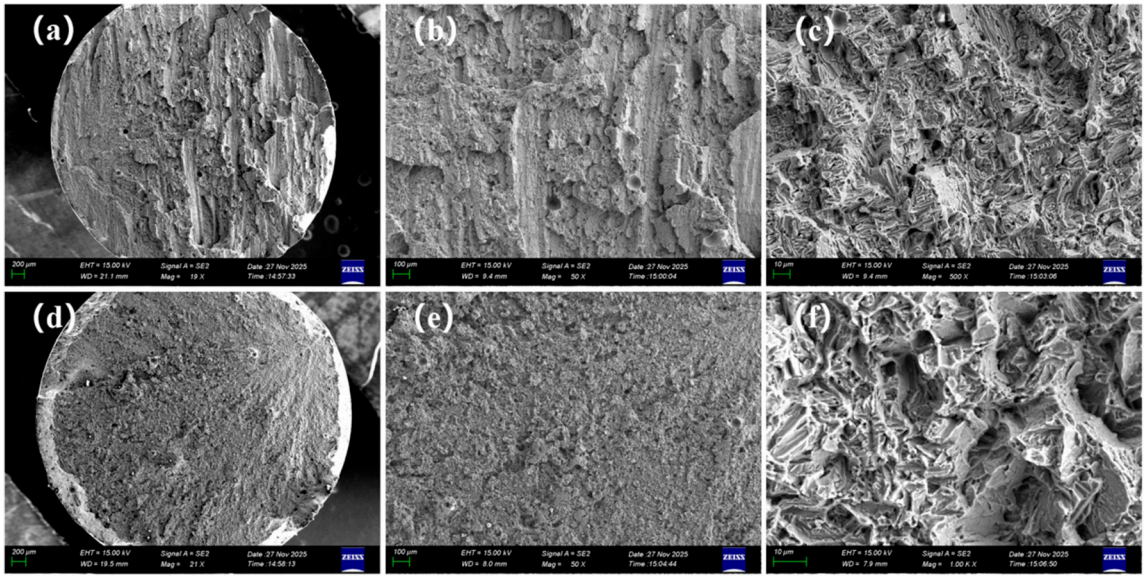


Figure 5. Room-temperature tensile fracture surfaces of specimens solution-treated at 1000 °C: (**a**–**c**) XY orientation, showing overall morphology and close-up details; (**d**–**f**) Z orientation, showing overall morphology and close-up details.

3.2.2. Tensile Tests at 650 °C and Fracture Surface Observations

The elevated-temperature tensile properties of different specimens are summarized in Table 5 and are plotted in Figure 6, respectively. At 650 °C, the strength of all specimens decreased compared with that at room temperature, whereas the ductility increased markedly. The elongation in the Z direction was generally higher than that in the XY direction. The as-built specimen exhibited a UTS of approximately 550 MPa and a YS of approximately 430 MPa in both the XY and Z directions, with elongations of approximately 15% and 26.5%, respectively. After 800 °C/2 h + 650 °C/2 h treatment, the Z-direction elongation increased to the highest value of approximately 44.5%, while the XY-direction elongation was about 18.8%. After 900 °C treatment, the XY-direction UTS increased to approximately 584 MPa, but the elongation decreased to approximately 10.5%; the Z-direction elongation remained at about 34.5%. After 1000 °C/2 h + 650 °C/2 h treatment, the XY-direction UTS and YS reached approximately 608 MPa and 468 MPa, respectively. After 1000 °C/4 h + 650 °C/2 h treatment, the XY-direction UTS increased to approximately 614 MPa, while the Z-direction elongation was approximately 31%. Extending the aging time at 650 °C further increased the yield strength. After aging for 8 h, the XY-direction UTS and YS reached approximately 617 MPa and 497 MPa, respectively, while the Z-direction elongation remained at about 26%. Overall, the 800 °C treatment is most beneficial for elevated-temperature ductility, whereas 1000 °C/2 h + 650 °C/4–8 h and 1000 °C/4 h + 650 °C/2 h provide a superior combination of strength and ductility at elevated temperature.

Table 5. Data from tensile tests of the EB-PBF Ti65 alloy under different heat-treatment conditions at 650 °C, including yield strength, ultimate tensile strength, and elongation.

Heat Treatment Conditions	Building Direction	UTS (MPa)	YS (MPa)	Elongation (%)
As-built	XY	555	428	12.5
As-built	XY	552	433	17.5
As-built	Z	554	429	26
As-built	Z	546	426	27

Table 5. *Cont.*

Heat Treatment Conditions	Building Direction	UTS (MPa)	YS (MPa)	Elongation (%)
800 °C/2 h + 650 °C/2 h	Z	566	428	42.5
800 °C/2 h + 650 °C/2 h	Z	568	426	46.5
800 °C/2 h + 650 °C/2 h	XY	560	422	22.5
800 °C/2 h + 650 °C/2 h	XY	565	424	15
900 °C/2 h + 650 °C/2 h	Z	572	444	34.5
900 °C/2 h + 650 °C/2 h	Z	572	428	34.5
900 °C/2 h + 650 °C/2 h	XY	583	433	11.5
900 °C/2 h + 650 °C/2 h	XY	585	436	9.5
1000 °C/2 h + 650 °C/2 h	Z	563	448	23.5
1000 °C/2 h + 650 °C/2 h	Z	592	463	25
1000 °C/2 h + 650 °C/2 h	XY	605	460	10.5
1000 °C/2 h + 650 °C/2 h	XY	612	477	14.5
1000 °C/4 h + 650 °C/2 h	Z	595	454	26.5
1000 °C/4 h + 650 °C/2 h	Z	600	465	35.5
1000 °C/4 h + 650 °C/2 h	XY	615	455	16.5
1000 °C/4 h + 650 °C/2 h	XY	614	475	19
1000 °C/2 h + 650 °C/4 h	Z	584	476	16.5
1000 °C/2 h + 650 °C/4 h	Z	582	469	22
1000 °C/2 h + 650 °C/4 h	XY	607	471	20.5
1000 °C/2 h + 650 °C/4 h	XY	606	479	20.5
1000 °C/2 h + 650 °C/6 h	Z	585	475	16.5
1000 °C/2 h + 650 °C/6 h	Z	592	476	16.5
1000 °C/2 h + 650 °C/6 h	XY	602	496	9
1000 °C/2 h + 650 °C/6 h	XY	603	490	17
1000 °C/2 h + 650 °C/8 h	Z	601	481	23.5
1000 °C/2 h + 650 °C/8 h	Z	602	491	28.5
1000 °C/2 h + 650 °C/8 h	XY	617	497	15
1000 °C/2 h + 650 °C/8 h	XY	616	497	15

The high-temperature tensile fracture surfaces of specimens subjected to solution heat treatment at 900 °C are provided in Figure S4 of the Supporting Information. As presented in Figure S4a–c, the high-temperature fracture surface of the XY-oriented specimens exhibits a mixed-mode ductile fracture, characterized by abundant dimples and partially retained columnar grain boundaries, along with a small number of cleavage facets and void defects. As depicted in Figure S4d–f, the high-temperature fracture surface of the Z-oriented specimens displays transgranular ductile fracture, predominantly covered with numerous dimples, accompanied by minor cleavage facets and void defects.

Figure 7 illustrates the high-temperature tensile fracture surfaces of specimens after solution heat treatment at 1000 °C. As shown in Figure 7a–c, the high-temperature fracture surface of the XY-oriented specimens remains a mixed-mode ductile fracture, featuring abundant dimples, partially retained columnar grain boundaries, and a limited number of cleavage facets and void defects. As illustrated in Figure 7d–f, the high-temperature fracture surface of the Z-oriented specimens exhibits transgranular ductile fracture, primarily consisting of extensive dimple structures, together with sporadic cleavage facets and void defects. Compared with the high-temperature fracture surfaces of specimens solution-treated at 800 °C and 900 °C, the dimples on the fracture surface of the 1000 °C specimen are generally larger. This observation is attributed to the bimodal distribution of the α phase and the coarsening of the primary α phase resulting from the 1000 °C solution treatment.

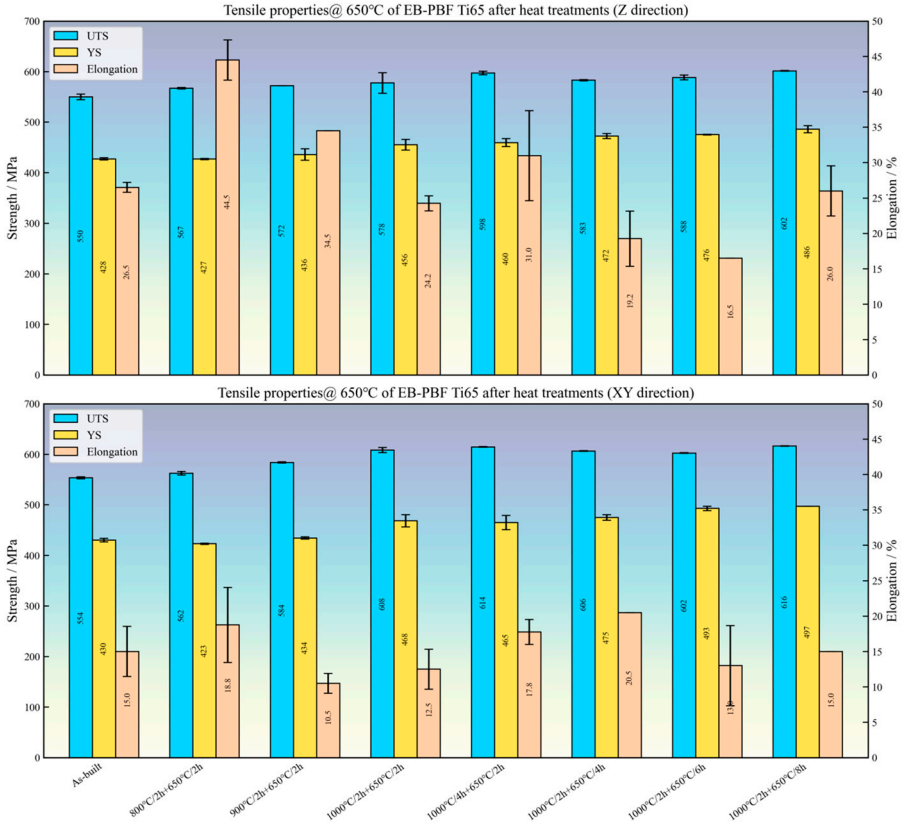


Figure 6. Tensile properties of the EB-PBF Ti65 alloy under different heat-treatment conditions at 650 °C, including yield strength, ultimate tensile strength, and elongation.

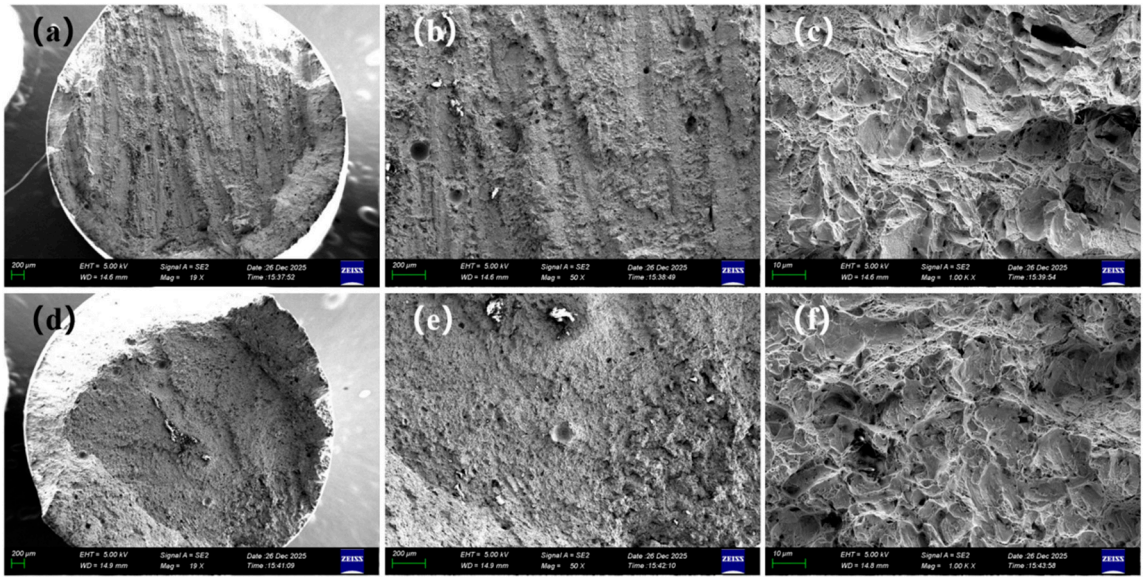


Figure 7. Tensile fracture surfaces at 650 °C of specimens solution-treated at 1000 °C: (**a**–**c**) XY orientation, showing overall morphology and close-up details; (**d**–**f**) Z orientation, showing overall morphology and close-up details.

4. Discussion

4.1. Effect of Solution Heat Treatment

The solution temperature is a critical factor dictating the microstructural morphology, phase composition, and mechanical properties of the additively manufactured Ti65 alloy. As a near-α high-temperature titanium alloy, the strengthening mechanisms of Ti65 primarily

stem from the refinement of the α/β lamellar microstructure, solid solution strengthening of the α phase, and dispersion strengthening via the precipitation of fine secondary α phase and silicides during aging. For the electron beam powder bed fusion (EB-PBF) fabricated specimens, rapid solidification coupled with layer-by-layer thermal cycling induces a fine, dense basketweave α + β lamellar microstructure, while simultaneously retaining a certain degree of residual stress, microstructural orientation, and interlayer variations.

As revealed by the DSC curve(see Figure 8), the EB-PBF Ti65 alloy exhibits a distinct thermal effect zone (endothermic region) during the heating process. The characteristic temperatures are identified as an onset temperature of ~887.5 °C, a peak temperature of ~894.8 °C, and an end temperature of ~950.9 °C. This temperature range is considered to correspond to the decomposition of metastable microstructures, the dissolution of the lamellar α phase, and the accelerated initiation of the α→β phase transformation. In the EB-PBF Ti65 alloy, rapid solidification and multiple thermal cycles not only yield the fine basketweave α + β lamellae but also induce localized elemental microsegregation, residual stresses, and a high density of defects. Consequently, during heating, the fine α lamellae, metastable β phase, or localized β-stabilizer-enriched regions preferentially undergo recovery, elemental redistribution, and phase transformation, giving rise to the thermal effect peak at approximately 890 °C. This peak does not necessarily represent the absolute β-transus temperature; rather, it more likely reflects the comprehensive thermal effects associated with the significant onset of α-phase dissolution, the rapid increase in β-phase fraction, and the microstructural transition from stable lamellae to a high-temperature α + β state. For the near-α Ti65 alloy, the primary phase transformation occurs above ~900 °C. Approaching 1000 °C, the α phase undergoes massive dissolution as the microstructure transitions into the high-temperature β-phase field. Due to the rapid cooling rates and complex thermal cycling inherent to the EB-PBF process, the microstructure is exceptionally fine and exhibits non-equilibrium elemental distributions. This may slightly lower the onset temperature of the phase transformation and result in a broader, flatter thermal effect peak. Furthermore, the fine lamellar α phase in the as-built microstructure possesses a large interfacial area and short diffusion distances, making it more susceptible to dissolution and elemental redistribution during heating. Thus, the phase transformation may initiate earlier compared to conventionally forged or cast materials. On the other hand, the localized segregation of Al-rich or β-stabilizer-rich regions can lead to inhomogeneous phase transformation temperatures across different regions, further broadening the DSC peak rather than forming a sharp, single peak. Therefore, the selection of 800 °C, 900 °C, and 1000 °C for solution treatments is highly justified: 800 °C corresponds to the pre-transformation recovery and stress-relief stage; 900 °C approaches the active phase transformation regime, promoting α-lamellae adjustment and partial β-phase formation; 1000 °C is near or within the high-temperature α + β transformation zone, significantly driving microstructural reconstruction and the reprecipitation of strengthening phases.

Figure 9b displays the EDS elemental distribution of the specimen solution-treated at 800 °C. Similar to the as-built state (Figure 9a), the β phase is primarily enriched in W, Si, Ta, and Mo. Additionally, localized segregation spots of Zr, W, Si, Ta, and Nb are present within the β phase; these elemental enrichments correspond to silicides located at the α/β phase interfaces. However, when the solution temperature is increased to 1000 °C (Figure 9c), although the β phase remains enriched in W, Si, Ta, and Mo, the previously observed elemental segregation spots completely disappear, indicating a uniform elemental distribution following high-temperature solution homogenization.

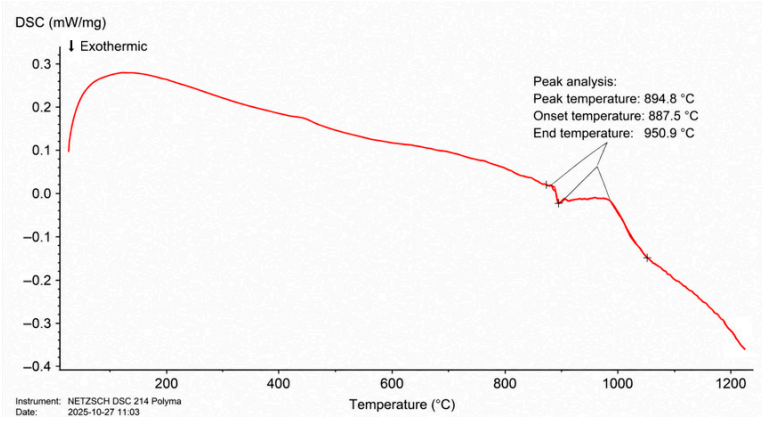


Figure 8. DSC testing results of the as-built EB-PBF Ti65 alloy.

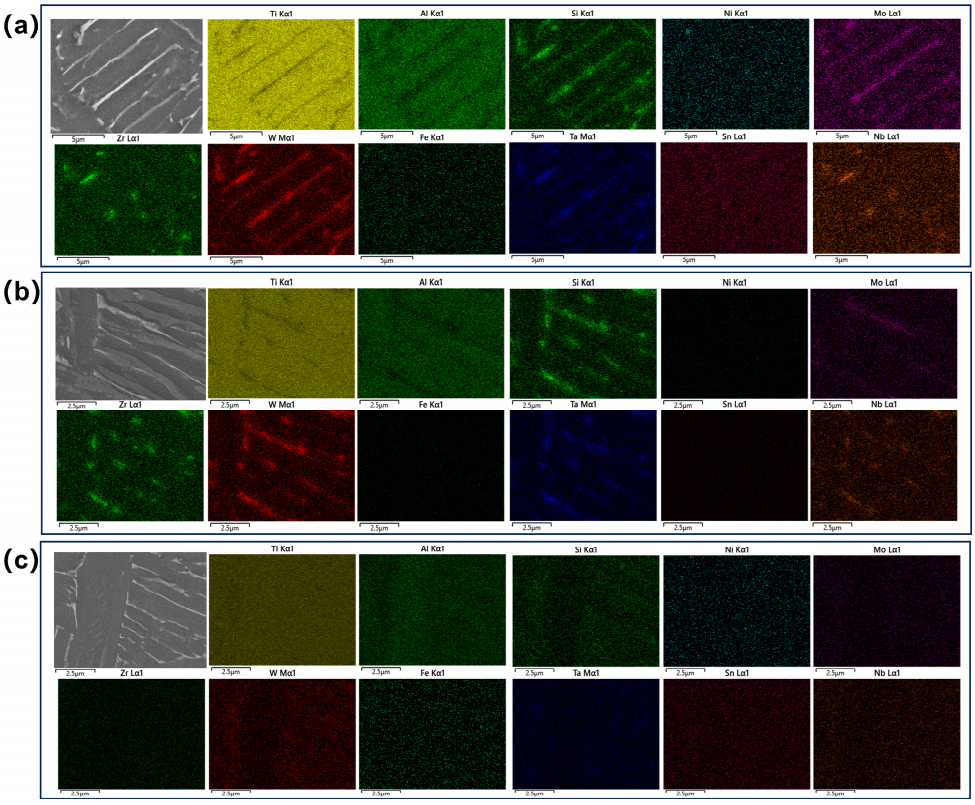


Figure 9. EDS analysis results of the EB-PBF Ti65 alloy under different heat treatment regimes: (**a**) as-built state; (**b**) 800 °C/2 h + 650 °C/2 h; (**c**) 1000 °C/2 h + 650 °C/2 h.

At a solution temperature of 800 °C, which is relatively low and well below the β-transus temperature, the microstructure remains dominated by the original as-built fine α lamellae, with limited dissolution and reconstruction of the α phase. The heat treatment at this temperature primarily manifests as recovery, residual stress relief, and localized compositional homogenization, rather than significantly altering the lamellar morphology. Consequently, the room-temperature tensile strength shows negligible changes compared to the as-built state, and the improvement in XY-direction ductility is limited. This indicates that the influence of the original melt pool boundaries, interlayer microstructural variations, and lamellar orientations on transverse deformation persists. However, during high-temperature tensile testing at 650 °C, the 800 °C solution-treated specimens exhibit an outstanding ductility advantage, with the Z-direction elongation at fracture reaching its highest level. This suggests that preserving the fine lamellar microstructure while

appropriately reducing internal stresses facilitates the activation of multiple slip systems and deformation compatibility at elevated temperatures, thereby mitigating the propensity for early cracking. Therefore, the significance of the 800 °C solution treatment lies in enhancing microstructural stability and high-temperature deformability without severely sacrificing strength, making it particularly suitable for service environments demanding high elevated-temperature ductility.

When the solution temperature is elevated to 1000 °C, the heat treatment effects change significantly. This higher temperature induces partial dissolution, fragmentation, and reprecipitation of the original fine α lamellae. The boundaries of the lamellar colonies become highly distinct, microstructural homogeneity is markedly improved, and residual stresses are further relieved. Under high-temperature solution conditions approaching the β-transus, the fraction of the β phase increases, and alloying elements are redistributed between the α and β phases. During subsequent cooling and aging, more stable lamellar α and fine secondary α phases precipitate, achieving a synergistic effect of solid solution strengthening and precipitation strengthening. The high-temperature solution treatment thus effectively mitigates the microstructural directionality and localized stress concentrations inherent to the as-built state, thereby endowing the alloy with a superior strength-ductility synergy at room temperature (Section 3.2.1). At 650 °C, the 1000 °C solution-treated specimens also exhibit higher XY-direction strength than the low-temperature solution-treated specimens (Section 3.2.2), indicating that this regime is highly beneficial for enhancing high-temperature load-bearing capacity.

It is worth noting that the 1000 °C solution treatment also carries risks of microstructural coarsening and plasticity fluctuations. If the holding time is too short, insufficient localized microstructural homogenization, combined with defects, coarse lamellae, or continuous grain boundary α phase, may lead to scatter in the high-temperature ductility of individual Z-direction specimens. If the holding time is extended to 4 h, compositional diffusion is more adequate, and residual stresses are more thoroughly relieved, leading to improved high-temperature ductility stability. However, excessive holding can cause coarsening of the α lamellae and lamellar colonies, weakening the fine-grain/fine-lamellae strengthening effect and degrading room-temperature ductility in certain directions. Therefore, the key to the 1000 °C solution treatment lies in striking a balance between microstructural reconstruction and lamellar coarsening.

In summary, the 800 °C treatment is advantageous for preserving fine lamellae and enhancing high-temperature ductility; the 900 °C treatment increases strength but offers limited improvement in anisotropy; the 1000 °C treatment significantly homogenizes the microstructure, enhances strength, and improves comprehensive room-temperature properties, representing the optimal temperature range for tailoring the heat treatment regime of the additively manufactured Ti65 alloy. Nevertheless, to avert lamellar coarsening and plasticity fluctuations, it must be coupled with an appropriate holding time and a rational 650 °C aging regime to achieve the optimal combination of strength, high-temperature ductility, and microstructural stability.

4.2. Effect of Aging Heat Treatment

After solution treatment, a certain amount of β phase and supersaturated solute elements are retained in the microstructure of the Ti65 alloy. During aging at 650 °C, the β-stabilizing elements in the β phase are redistributed, and fine secondary α phase, silicides, and other dispersed precipitates gradually form. These precipitates can effectively impede dislocation motion, thereby increasing the yield strength and elevated-temperature load-bearing capacity.

When the aging duration is 2 h, the precipitation process is still in its initial stage. The number density of fine secondary α precipitates is limited, and the precipitation strengthening effect has not yet been fully activated. Therefore, although the alloy exhibits relatively high ultimate tensile strength, the improvement in yield strength remains limited. In addition, some Z-direction specimens show considerable scatter in ductility during tensile testing at 650 °C, indicating that short-time aging is insufficient to fully stabilize the non-equilibrium microstructure and local compositional fluctuations produced after solution treatment.

As the aging duration is extended to 4 h, elemental diffusion and precipitation become more complete. The number density of secondary α phase and dispersed silicides increases, and their distribution becomes more homogeneous, enabling the alloy to achieve a favorable strength–ductility balance (Section 3.2.2). This indicates that moderate aging enhances the obstruction to dislocation motion without inducing obvious embrittlement.

When the aging duration is further prolonged to 6 h, the yield strength continues to increase, whereas the elongation after fracture decreases. This suggests that the increased amount of precipitates and enhanced α/β interfacial strengthening improve the resistance to plastic deformation, but simultaneously reduce the capacity for dislocation slip and interfacial deformation compatibility, thereby promoting strain localization.

After aging for 8 h, the strength reaches its highest level among the investigated conditions. Meanwhile, the Z-direction specimens still retain relatively good ductility, indicating that the precipitates gradually become stable and the thermal stability of the microstructure is enhanced. Nevertheless, excessively prolonged aging may also induce coarsening of the α lamellae or precipitates, thereby weakening the ductility reserve.

In summary, aging for 4 h is more favorable for achieving a balanced combination of strength and ductility, whereas aging for 6–8 h is more suitable for service conditions requiring high elevated-temperature strength and microstructural stability. For the EB-PBF Ti65 alloy, the appropriate aging duration should be selected according to service requirements by balancing strength, ductility, and thermal stability.

4.3. Comparison with Previous Studies

To place the present findings in the context of previous studies on additively manufactured Ti65 alloy, the microstructures and tensile properties obtained in this work are compared with representative literature results in Table 6 and the following paragraphs. In terms of microstructure, the as-built EB-PBF Ti65 alloy exhibits a fine basketweave α + β lamellar microstructure, which differs from the hierarchical α′ martensite typically formed in laser powder bed fusion (LPBF) fabricated Ti65 [4] and from the coarse columnar prior-β grains with a strong [0001] texture along the deposition direction reported for laser directed energy deposition (LDED) fabricated Ti65 [15]. This difference arises from the high-temperature preheating and intrinsic cyclic thermal history of the EB-PBF process, which promotes in situ decomposition of martensitic constituents and yields a fine, near-equilibrium lamellar morphology. After the 1000 °C solution treatment, the continuous grain-boundary α phase becomes discontinuous and a bimodal-like α morphology develops. This evolution is consistent with the observations of Sun et al. [15], in which annealing LDED Ti65 at 950 °C produced a trimodal microstructure with discontinuous grain-boundary α and markedly improved tensile isotropy, and with those of He et al. [13], in which solution-plus-aging treatment of laser-deposited Ti65 generated a duplex microstructure with improved plasticity. The agreement between these independent studies indicates that disrupting the continuity of grain-boundary α through sub-transus solution treatment is a general and effective microstructural tailoring route for additively manufactured near-α titanium alloys.

Table 6. Comparison of tensile properties of the Ti65 alloy fabricated by different additive manufacturing processes. Note: RT denotes room temperature; the present data are mean values; the elevated-temperature data of Ref. [4] were measured at 600 °C.

Process	Post-Treatment	Test Temperature	UTS (MPa)	YS (MPa)	Elongation (%)	Reference
EB-PBF	As-built	RT	966	884	5.4 (XY)/13.1 (Z)	This work
EB-PBF	1000 °C/2 h + 650 °C/2 h	RT	~1050	~950	11.5 (XY)/12.9 (Z)	This work
EB-PBF	1000 °C/2 h + 650 °C/4 h	650 °C	607	475	20.5 (XY)	This work
Conventional LPBF	As-built	RT	1394	1113	7.1	[4]
Micro-LPBF	As-built	RT	1514	1297	4.5	[4]
Conventional LPBF	As-built	600 °C	826	760	10.0	[4]

In terms of mechanical properties, the present heat-treated EB-PBF Ti65 alloy achieves a room-temperature UTS of approximately 1050 MPa with an XY-direction elongation of 11.5%, whereas the as-built conventional LPBF Ti65 exhibits a higher UTS of 1394 MPa but a lower elongation of 7.1% owing to its fine α' martensitic microstructure [4]. The present 1000 °C/2 h + 650 °C/2 h treatment therefore provides a more balanced strength-ductility combination, together with an approximately 53% reduction in anisotropy relative to the as-built state. At elevated temperature, the present alloy retains a UTS of approximately 607 MPa at 650 °C with an elongation of 20.5%. For comparison, the as-built conventional LPBF Ti65 exhibits a UTS of 826 MPa at 600 °C [4]; considering that the present tests were conducted at the higher temperature of 650 °C and that the strength of near-α titanium alloys decreases markedly with increasing test temperature, the elevated-temperature strength retention of the heat-treated EB-PBF Ti65 is within a competitive range. Moreover, the aging-time dependence observed in this work is qualitatively consistent with the thermal-exposure behavior of forged Ti65 reported by Li et al. [21], in which the 650 °C tensile strength remained essentially stable while the ductility varied with exposure duration, confirming that aging-induced precipitation governs the strength-ductility balance at the service temperature. Overall, the recommended regime of 1000 °C/2 h + 650 °C/2–4 h delivers a combination of room-temperature strength, elevated-temperature strength retention, and reduced anisotropy that is comparable to or more balanced than those reported for additively manufactured Ti65 alloys fabricated by laser-based routes.

5. Conclusions

For the EB-PBF-fabricated Ti65 alloy, this study demonstrates that heat treatment significantly influences microstructure and mechanical properties. The as-built microstructure exhibits mechanical anisotropy primarily associated with the continuous grain-boundary alpha phase and oriented lamellar colonies. Solution treatment at 1000 °C for 2 h (below the beta-transus temperature of ~1010 °C) effectively promotes the discontinuous transformation of continuous grain-boundary alpha and facilitates bimodal alpha microstructure formation, resulting in room-temperature UTS of approximately 1050 MPa and XY-direction elongation increasing from 5.4% to 11.5%, corresponding to an anisotropy reduction of approximately 53%. At 650 °C, the 1000 °C/2 h + 650 °C/4 h treatment provides a favorable strength-ductility combination with XY-direction UTS of ~607 MPa and elongation of ~20.5%. The recommended heat-treatment regime of 1000 °C/2 h + 650 °C/2–4 h offers a balanced combination of room-temperature strength, elevated-temperature performance, and reduced anisotropy, making it suitable for aerospace applications requiring high-temperature load-bearing capacity and dimensional stability. Future work should include quantitative phase-fraction analysis (e.g., XRD, TEM) and fracture-surface characterization

to further elucidate the mechanisms governing anisotropy reduction and high-temperature property optimization.

Supplementary Materials: The following supporting information can be downloaded at https://www.mdpi.com/article/10.3390/met16091021/s1. Figure S1: Optical micrographs (lower magnification) of the EB-PBF-fabricated Ti65 alloy subjected to various heat treatment regimes; Figure S2: SEM micrographs (lower magnification) of the EB-PBF-fabricated Ti65 alloy subjected to various heat treatment regimes; Figure S3: Room-temperature tensile fracture surfaces of specimens solution-treated at 900 °C; Figure S4: 650 °C tensile fracture surfaces of specimens solution-treated at 900 °C.

Author Contributions: Conceptualization, Y.J.; methodology, Y.J., Y.L., X.Z., F.G. and C.H.; validation, Y.J., Y.L., X.Z., F.G., C.H., Y.Z., J.Z. and Y.D.; formal analysis, Y.J., Y.L., X.Z., F.G., C.H., Y.Z., J.Z. and Y.D.; investigation, Y.J., Y.L., X.Z., F.G., C.H., Y.Z., J.Z. and Y.D.; resources, X.L.; data curation, Y.J.; writing—original draft preparation, Y.J., Y.Z. and J.Z.; writing—review and editing, X.L.; visualization, X.L.; project administration, Y.L.; funding acquisition, X.L. All authors have read and agreed to the published version of the manuscript.

Funding: This research was funded by the Defense Industrial Technology Development Program, grant number JCKY2023110A003.

Data Availability Statement: The data presented in this study are available on request from the corresponding author due to the inclusion of confidential data and proprietary information provided by third-party collaborators.

Acknowledgments: During the preparation of this manuscript/study, the authors used GPT-5.5 for the purposes of language editing and grammar check. The authors have reviewed and edited the output and take full responsibility for the content of this publication.

Conflicts of Interest: Author Yinling Jin, Yanmei Liu, Xingwang Zhao, Feng Guan and Chengjie Huang were employed by Shenyang Aircraft Corporation. And author Yu Zhang, Jingling Zhang and Yufeng Ding were employed by Beijing Quick Beam Technology Co., Ltd. The remaining authors declare that the research was conducted in the absence of any commercial or financial relationships that could be construed as a potential conflict of interest.

References

1. Srivastava, M.; Jayakumar, V.; Udayan, Y.; Muthu, S.M.; Gautam, P.; Nag, A. Additive Manufacturing of Titanium Alloy for Aerospace Applications: Insights into the Process, Microstructure, and Mechanical Properties. *Appl. Mater. Today* **2024**, *41*, 102481. [CrossRef]
2. Su, J.; Jiang, F.; Teng, J.; Chen, L.; Yan, M.; Requena, G.; Zhang, L.-C.; Wang, Y.M.; Okulov, I.V.; Zhu, H.; et al. Recent Innovations in Laser Additive Manufacturing of Titanium Alloys. *Int. J. Extrem. Manuf.* **2024**, *6*, 032001. [CrossRef]
3. Kang, L.; Yang, C. A Review on High-Strength Titanium Alloys: Microstructure, Strengthening, and Properties. *Adv. Eng. Mater.* **2019**, *21*, 1801359. [CrossRef]
4. Meng, Y.; Wu, J.; Xu, Z.; Wang, X.; Chen, X. Comparison of Microstructure and Mechanical Properties of Ti65 Alloy Prepared by Micro and Conventional Laser Powder Bed Fusion. *Metals* **2026**, *16*, 419. [CrossRef]
5. Yin, J.; Li, P.; Li, X.; Guan, F.; Wu, J.; Wang, S.; Yang, G. Analysis of Room-Temperature/High-Temperature High-Cycle Fatigue Performance of Laser Additive Manufactured Ti65 Titanium Alloy. *J. Mater. Eng. Perform.* **2025**, *34*, 8594–8601. [CrossRef]
6. Yin, J.; Li, X.; Guan, F.; Li, P.; Yang, G. Research on Microstructure and High-Temperature Performance of Novel Ti65 Titanium Alloy with V-Groove Connection in Laser Additive Manufacturing. *Trans. Indian Inst. Met.* **2024**, *77*, 3627–3639. [CrossRef]
7. Liu, L.; Li, X.; Yin, J.; Wang, C.; Zhang, J.; Li, P. Laser Additive Manufactured V-Shaped and L-Shaped Ti65 Titanium Alloy Interfaces and High-Temperature Performance. *J. Mater. Eng. Perform.* **2026**, *35*, 1432–1447. [CrossRef]
8. Li, B.; Yang, Y.; Ren, Y.; Li, C.; Yang, G. Effect of Subphase Change Point Temperature Cyclic Heat Treatment on the Microstructure and Mechanical Properties of Ti65 High-Temperature Titanium Alloy Fabricated by Laser Deposition Manufacturing. *J. Mater. Res. Technol.* **2025**, *37*, 3998–4015. [CrossRef]
9. Zhao, D.; Fan, J.; Zhang, Z.; Liang, X.; Chen, Z.; Chen, Z.; Lai, M.; Tang, B.; Kou, H.; Wang, Q.; et al. Variant Selection Mechanism of α Phase Associated with Initial Texture and Cooling Rate in Near-α Titanium Alloy Ti65. *Mater. Charact.* **2025**, *223*, 114874. [CrossRef]

10. Kang, L.-W.; Jiang, S.-S.; Zhang, J.-Y.; Li, Y.; Shi, X.-Y.; Huang, C.-Q.; Peng, P.; Yang, S.; Han, Z.; Lu, Z. Thermohydrogen-Induced A→β Phase Transition and Interfacial Aggregation: A Diffusion Bonding Mechanism for Ti65 Alloy at Low Temperatures. *Rare Met.* **2026**, *45*, e70089. [CrossRef]
11. Yin, J.; Zang, J.; Liu, J.; Zhou, L. Modeling of Microstructure Evolution of Ti65 Alloy during High Temperature Compression. *Int. J. Interact. Des. Manuf.* **2026**, *20*, 2309–2333. [CrossRef]
12. Fan, J.; Zhao, D.; Chen, Z.; Zhang, Z.; Wang, J.; Tang, B.; Chen, Z.; Wang, Q.; Kou, H.; Li, J. Tailoring Texture in a Near-α Titanium Alloy: Insights from Strain Paths and Cooling Rate Influences. *J. Mater. Res. Technol.* **2024**, *30*, 1388–1402. [CrossRef]
13. He, B.; Sun, J.; Ren, Y.; Li, C.; Yang, G.; Li, X.; Ni, J. Effect of Heat Treatment on Microstructure and Mechanical Properties of Laser-Deposited Ti65 near-Alpha Titanium Alloy. *J. Mater. Res.* **2022**, *37*, 1464–1474. [CrossRef]
14. Zhao, D.; Fan, J.; Zhang, Z.; Wang, J.; Wang, Q.; Chen, Z.; Tang, B.; Kou, H.; Li, J. Influence of A+β Solution Treatments on Ti65 Ultrathin Sheets: Silicide Precipitation, Mechanical Behaviour and Novel $\{10\bar{1}1\}$ Twinning System. *Trans. Nonferrous Met. Soc. China* **2023**, *33*, 1098–1113. [CrossRef]
15. Sun, J.; Lu, H.; Liang, Y.; Zhang, H.; Luo, K.; Lu, J. Evolution of Microstructure and Mechanical Properties of Ti65 High-Temperature Titanium Alloy after Additive Manufacturing and Annealing. *Mater. Sci. Eng. A* **2024**, *913*, 147002. [CrossRef]
16. Sun, J.; Lu, H.; Liang, Y.; Luo, K.; Lu, J. Effects of Different Heat Treatment Temperatures on the Microstructure and Mechanical Properties of Additive Manufacturing Ti65 Alloys. *Mater. Charact.* **2025**, *219*, 114592. [CrossRef]
17. Wang, Y.-C.; Liu, J.-Y.; Liu, J.-R.; Li, W.-Y.; Zhang, B.; Zhang, G.-P. Effects of Thermal Exposure Temperature on Room-Temperature Tensile Properties of Ti65 Alloy. *Materials* **2024**, *17*, 4424. [CrossRef] [PubMed]
18. Lv, X.; Li, G.; Wang, K.; Fu, H. Microstructure and Mechanical Properties of Ti65 Titanium Alloy T-Joints Welded by Dual-Beam Laser. *J. Mater. Res. Technol.* **2025**, *37*, 3846–3856. [CrossRef]
19. Tammas-Williams, S.; Zhao, H.; Leonard, F.; Derguti, F.; Todd, I.; Prangnell, P. XCT Analysis of the Influence of Melt Strategies on Defect Population in Ti-6Al-4V Components Manufactured by Selective Electron Beam Melting. *Mater. Charact.* **2015**, *102*, 47–61. [CrossRef]
20. Sames, W.J.; List, F.A.; Pannala, S.; Dehoff, R.R.; Babu, S.S. The Metallurgy and Processing Science of Metal Additive Manufacturing. *Int. Mater. Rev.* **2016**, *61*, 315–360. [CrossRef]
21. Li, J.; Jiang, W.; Xia, C.; Deng, Y.; Gao, Y.; Yang, C. Microstructural Evolution and Subsequent Mechanical Properties of Ti65 Titanium Alloy during Long-Term Thermal Exposure. *Metals* **2024**, *14*, 854. [CrossRef]

Disclaimer/Publisher's Note: The statements, opinions and data contained in all publications are solely those of the individual author(s) and contributor(s) and not of MDPI and/or the editor(s). MDPI and/or the editor(s) disclaim responsibility for any injury to people or property resulting from any ideas, methods, instructions or products referred to in the content.